Spin Entanglement and Magnetic Competition via Long-Range Interactions in Spinor Quantum Optical Lattices

Karen Lozano-Méndez, Alejandro H. Cásares, and Santiago F. Caballero-Benítez*
Instituto de Física, LSCSC-LANMAC, Universidad Nacional Autónoma de México, Ciudad de México 04510, Mexico

(Received 16 November 2020; revised 20 December 2021; accepted 14 January 2022; published 22 February 2022)

Quantum matter at ultralow temperatures offers a test bed for analyzing and controlling desired properties in strongly correlated systems. Under typical conditions the nature of the atoms fixes the magnetic character of the system. Beyond classical light potentials leading to optical lattices and short-range interactions, high-Q cavities introduce novel dynamics into the system via the quantumness of light. Here we propose a theoretical model and we analyze it using exact diagonalization and density matrix renormalization group simulations. We explore the effects of cavity mediated long-range magnetic interactions and optical lattices in ultracold matter. We find that global interactions modify the underlying magnetic character of the system while introducing competition scenarios. Antiferromagnetic correlated bosonic matter emerges in conditions beyond what nature typically provides. These allow new alternatives toward the design of robust mechanisms for quantum information purposes, exploiting the properties of magnetic phases of strongly correlated quantum matter.

DOI: 10.1103/PhysRevLett.128.080601

Magnetic quantum matter in optical lattices offers a collection of interesting phenomena in terms of quantum simulation [1]. There are possible applications ranging from quantum computing protocols to quantum system design. These designs could help understand the underlying mechanisms that trigger different kinds of order in analog real materials. The matter is controlled with flexibility, generating effective synthetic quantum matter solids. The degree of precision achieved allows us to control the emergence of different quantum many-body phases. In these settings, strong quantum correlations are present, while paradigmatic scenarios of condensed matter systems regarding quantum phase transitions (QPT) are reproduced. Recent advances controlling ultracold matter allow the experimental realization of fermionic antiferromagnets [2–5]. These findings contribute to understand, via quantum simulation, some features linked to high-T_c superconductivity. In the typical setting, the light fields act parametrically like classical waves generating a "classical" optical lattice (COL). The state of the photons is not altered by the backaction of matter. Going beyond classical light fields by the inclusion of cavity backaction in an ultracold system takes matter into new regimes. Correlations induced by the high-Q cavity light to the matter and vice versa modify significantly the energy manifolds experienced by the matter [6]. Consequently, new correlated phases of matter can emerge. Ultracold systems without COL inside high-Q cavities with magnetic properties have been recently achieved by several groups with bosons and fermions [7–13]. Several proposals regarding exploiting these magnetic interactions without a lattice have been put forward with neutral atoms [14–17]. In this limit, the interplay between cavity light and internal degrees of freedom has been studied in combination with the dynamical and dissipative nature of the system. Recently, the inclusion of COL and cavity backaction was achieved [18–21]. In these experiments, the competition of different spatial orders is possible and COL can be controlled arbitrarily. Several studies have explored these setups and QPTs [22–31]. However, the interplay regarding magnetism in COL with cavity induced interactions, strong quantum correlations, and insulating states remains largely unexplored.

Here, we show how the interplay of magnetism, COL, and cavity induced magnetic interactions allow us to control the emergence of nontrivial magnetic phases of

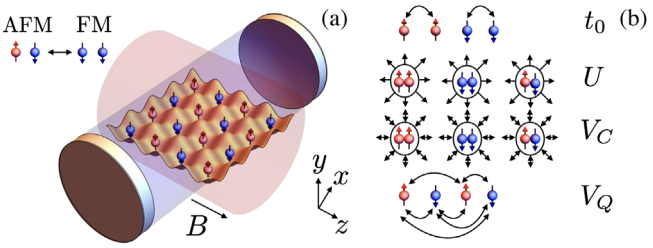

FIG. 1. Schematic of the system of ultracold atoms in a high-Q cavity with a COL and magnetic degrees of freedom. (a) Typical atomic antiferromagnet. The V_{OL} (lattice) with intracavity light $\hat{a}$ (cavity axis shade), pumped light (transverse shade) $\Omega_{z,p}$, and applied magnetic field B. (a) (top left) QPTs between AFM $\leftrightarrow$ FM are possible. (b) Effective atomic interaction processes for different spin components: tunneling amplitude t_0, on-site repulsion U, intrinsic (local) magnetic interaction V_C, and cavity induced (global) magnetic interactions V_Q.

quantum matter. Light and matter are entangled via the cavity generating effective magnetic global interactions. Therefore, quantum antiferromagnets (AFM) and ferromagnets (FM) can be produced efficiently. Thus, quantum state engineering of magnetic states with strong correlations can be optimized in a single setup and goes beyond what the nature of the atoms typically allows.

Effective spinor quantum optical lattice model.—We study ultracold bosonic atoms with $F = 1$ spin $\sigma \in \{\downarrow, 0, \uparrow\}$, trapped in a COL subject to a constant magnetic field such that the magnetic sublevels split inside a high-Q cavity. The alkali atoms in the COL have tunneling amplitude t_0, on-site repulsion with strength U, and local magnetic interactions (classical) $\propto V_C$. The Hamiltonian describing these processes without the cavity is the Spinor Bose-Hubbard Hamiltonian [1,32]. We refer to it as "spinor classical optical lattice" (SCOL) as the lattice potential comes from a classical treatment of light. The model is

$$\mathcal{H}_{\mathrm{SCOL}} = \mathcal{H}_U + \frac{V_C}{2}\sum_i (\hat{\mathbf{S}}_i^2 - 2\hat{n}_i), \tag{1}$$

with $\mathcal{H}_U = -t_0 \sum_{\sigma,\langle i,j\rangle} (\hat{b}_{i,\sigma}^\dagger \hat{b}_{j,\sigma} + \mathrm{H.c.}) + (U/2)\sum_i \hat{n}_i(\hat{n}_i - 1)$, The spin operators for $F = 1$ per site are $\hat{S}_{\nu,i} = \sum_{\xi,\xi'} \hat{b}_{\xi,i}^\dagger F_{\xi,\xi'}^\nu \hat{b}_{\xi',i}$, where $\nu \in \{x, y, z\}$ and F^ν, the angular momentum matrices. The $b_{\sigma,i}^\dagger(\hat{b}_{\sigma,i})$ correspond to bosonic atoms at site i and spin σ in the COL. The total spin per site is $\hat{\mathbf{S}}_i^2 = \sum_\nu \hat{S}_{\nu,i}^2$ and the particle number per site operator is $\hat{n}_i = \sum_\sigma \hat{n}_{\sigma,i}$. Additionally, the atoms are inside a single-mode high-Q cavity with the mode frequency ω_c and decay rate κ in off-resonant scattering Fig. 1. Linearly polarized laser light is pumped into the cavity with the Rabi frequency $\Omega_{z,p}(\mathbf{B})$ dependent on the applied magnetic field $\mathbf{B} = B\hat{e}_z$ [33] and frequency $\omega_p(\Delta_c = \omega_p - \omega_c)$. The atoms are illuminated from an axis perpendicular to the cavity axis in a standing wave configuration. Each spin component couples with the cavity mode via the effective coupling strength $\tilde{g}_z = g J_z \Omega_{z,p}\sqrt{N_s}/\Delta_a$, with the light-matter coupling coefficient g, and the detuning between the light and atomic resonance $\Delta_a = \omega_p - \omega_a$ [34]. In the COL basis (Wannier basis), the atoms experience the projection of the cavity light mode with amplitude J_z over N_s sites [33]. For simplicity, the COL is deep enough such that cavity-induced tunneling amplitudes (long-range bond processes) are neglected and only COL nearest-neighbor tunneling remains [23,35]. Experimentally, this is possible in the nonmagnetic version of our system [19]. The Hamiltonian of the light-matter system is $\mathcal{H} = \mathcal{H}_{\mathrm{SCOL}} + \mathcal{H}^a + \mathcal{H}^{ab} + \mathcal{H}_B$. The cavity light Hamiltonian is $\mathcal{H}^a = -\hbar\Delta_c \hat{a}^\dagger \hat{a}$, the operators $\hat{a}^\dagger$ ($\hat{a}$) create (annihilate) photons. The applied magnetic field term is $\mathcal{H}_B = \mu_B g_S \sum_i \hat{\mathbf{S}}_i \cdot \mathbf{B}$ with g_S the effective Landé factor [36]. The light-atom magnetic interaction ($\mathcal{H}^{ab}$) is controlled using the vectorial components of the polarizability encoded in $\Omega_{z,p}$ [7,9,33,36]. The light-matter interaction is generalized to the lattice case by expanding in the Wannier basis [37,38],

$$\mathcal{H}^{ab} = \frac{\hbar}{\sqrt{N_s}}\sum_i (\tilde{g}_z \varphi_{z,i}\hat{a}^\dagger + \tilde{g}_z^* \varphi_{z,i}^* \hat{a})\hat{S}_{z,i}. \tag{2}$$

The function $\varphi_{z,i}$ encodes the mode structure of the light into the matter [33]. This depends on the pump incidence angle with respect to the cavity axis and COL plane [23]. Considering the experimental situation described in Ref. [7] without COL, the couplings of the "x" and "y" components of the angular momentum are neglected due to energetic considerations, as $|\hbar\Delta_c| \ll \mu_B B$ [33]. Similar decompositions are possible in analog Fermi systems ($S = 1/2$) [39–41]. In general, the spatial structure of the light modes gives a natural basis for collective modes [23]. For simplicity, we neglected the nonvectorial (nonmagnetic) contributions of the polarizability. Moreover, we take $|\hbar\Delta_a| \gg \hbar\kappa, |\hbar\Delta_c|$ to avoid heating and $\hbar\kappa, |\hbar\Delta_c| \gg t_0$ to avoid nonadiabatic effects in the atomic lattice dynamics [42], and $\kappa \ll |\Delta_c|$. Nonadiabatic effects are minimized in experiments under these assumptions [7]. We adiabatically eliminate the cavity light following Ref. [42]. This amounts to effectively integrate out the light. Qualitatively, $\langle \dot{\hat{a}} \rangle = 0$, then it follows, $\langle \hat{a} \rangle \sim \sum_i \langle \tilde{g}_z \varphi_{z,i} \hat{S}_{z,i} \rangle$. Beyond this limit, nonadiabatic effects modify slightly the emergence of superfluid (SF) phases. However, insulating states are robust, but effective renormalization of parameters due to cavity noise effects is needed [43]. We find an effective "spinor quantum optical lattice" (SQOL),

$$\mathcal{H}_{\mathrm{SQOL}} = \mathcal{H}_{\mathrm{SCOL}} + \frac{V_Q}{N_s}\sum_{i,j} f_{i,j}^\varphi \hat{S}_{z,i}\hat{S}_{z,j}, \tag{3}$$

where $\mathcal{H}_B$ has been effectively decoupled from the low energy atomic dynamics but fixes the quantization axis. We call the model "quantum" as the cavity induced interaction depends on the quantum state of light and the backaction of the quantum state of matter [23]. Here $f_{i,j}^\varphi = \mathrm{Re}(\varphi_{z,i}^* \varphi_{z,j})$, $V_Q = \hbar\Delta_c |\tilde{g}_z|^2/(\Delta_c^2 + \kappa^2)(1 + \kappa_{\mathrm{nad}})$, and nonadiabatic corrections are $\kappa_{\mathrm{nad}} = -\kappa^2/\Delta_c^2$ [44]. κ_{nad} shows that photon loses need to be minimized to control $\mathrm{sign}(\Delta_c)$. Stability of photon steady states ($\Delta_c > 0$) is sensitive to atomic deconfinement temperature effects. Metastable states are possible for $\Delta_a > 0$. Photon steady states with either sign of Δ_c were achieved in ms [21]. The matter will self-organize in such a way that the cavity induced interaction components "i, j" are maximized (minimized) by $f_{i,j}^\varphi \Delta_c > 0$ ($f_{i,j}^\varphi \Delta_c < 0$), as cavity light maximizes (minimizes) akin to superradiance (subradiance). For minimized cavity light, quantum fluctuations play a fundamental

role [23,38]. The number of photons in the cavity is $n_{\rm ph} = \langle \hat{a}^\dagger \hat{a} \rangle \approx |V_Q/(N_s \Delta_c) \sum_{i,j} f^{\varphi}_{i,j} \langle \hat{S}_{z,i} \hat{S}_{z,j} \rangle|$. In addition, there is competition between the typical local (short-range) processes in the Bose-Hubbard model ($\propto U$ and t_0), "local" spin classical interactions ($\propto V_C$) and the "global" (long-range) cavity induced spin quantum interactions ($\propto V_Q$). Their interplay leads to different quantum critical points (QCPs). Typical frequencies of the analogous system without COL are $\kappa \ll |\Delta_c| \sim$ MHz and $E_R \sim h \times 4$ kHz, E_R being the recoil energy [7]. Typical values of the nonmagnetic system with COL are $t_0 \sim E_R$ and $\Delta_a \sim$ 10–100 GHz [21]. In the case of SCOL ($V_Q = 0$), the sign of the magnetic interaction V_C is fixed by the nature of the atom to be either ferromagnetic for $V_C < 0$ or antiferromagnetic for $V_C > 0$. Typical atoms used are ^{87}Rb (F), ^{7}Li (F), or ^{23}Na (AFM) with $V_C/U \sim (-0.005, -0.23, 0.04)$ [32]. In the system with $V_Q \neq 0$, parameters can be tuned externally (i.e., Δ_c) triggering different magnetic behavior. We study configurations $[\phi_\pm = \varphi_{z,i} = (\pm 1)^i]$, where the pump incidence angle maximizes diffraction generating homogenous coupling (ϕ_+) or staggered density coupling in the diffraction minima (ϕ_-) similar to current experimental settings. Tuning noninsulating antiferromagnetic and ferromagnetic states with ϕ_- is experimentally feasible [7]. More elaborate scenarios and flexibility can be achieved depending on the pumps, the cavity setup, and the magnetic field [6,23,38,45].

Magnetic interactions.—It is experimentally possible to prepare the system with different spin populations without the lattice in the cavity [7]. Without the cavity with COL, the phase diagram is well known [1,32,46], having polar, FM, and AFM phases. We choose commensurate fillings in the lattice to study the behavior between Mott-insulator (MI) phases driven by U and the magnetic dynamics. In the effective model for convenience, we introduce linear $\epsilon_{\uparrow\downarrow} \sum_i \hat{S}_{z,i}$ (quadratic, $\epsilon_0 \sum_i \hat{n}_{0,i}$) magnetic field shift favoring (suppressing) one of the spin components "$\uparrow\downarrow$" ("0") relevant for FM (AFM) ordering, ϵ_σ a small perturbation [32]. In the case where $V_C = 0$ the behavior is simplified as the "0" component decouples due to the interaction form. The many-body quantum state is $|\Psi\rangle = |\Psi_0\rangle \otimes |\Psi_{\uparrow,\downarrow}\rangle$ [33]. For simplicity in what follows, we consider $\epsilon_0 > 0$, suppressing polar configurations. Preparing the system with the 0 component empty is experimentally achievable [7].

Cavity induced ferromagnetic configurations (V_C=0).—The behavior is intuitive for ϕ_+ and $V_Q < 0$, the system maximizes either spin component $\uparrow\downarrow$ depending on the sign of $\epsilon_{\uparrow\downarrow} \neq 0$ having a ferromagnet. Similarly, for ϕ_-, $V_Q > 0$, the system is always FM. In these cases, the system behaves as a single component Bose-Hubbard model either $\uparrow\downarrow$. The ground state is magnetically trivial being fully polarized [47]. The system goes from FM insulator (FMI) to F superfluid (FMSF) increasing t_0/U.

Cavity induced antiferromagnetic correlations ($V_C = 0$).—Notably, if $V_Q < 0, \phi_-$ or $V_Q > 0, \phi_+$, the situation is not magnetically trivial as AFM correlations emerge. The system is a balanced mixture $\sum_i \langle \hat{n}_{\uparrow,i} \rangle = \sum_i \langle \hat{n}_{\downarrow,i} \rangle$. However, the total population fluctuations per site $(\Delta(\hat{n}_i)^2 = \langle \hat{n}_i^2 \rangle - \langle \hat{n}_i \rangle^2)$ for large U are minimized as the Mott gap ($\Delta_e = U$) opens. The MI state exhibits large fluctuations per site in the $\uparrow\downarrow$ components. The system goes from an AFM insulator (AFMI) to a paramagnetic SF (PSF) as t_0/U increases [33].

Deep Mott insulator limit AFMs ($U \gg t_0$, $V_C = 0$).—We study the spin quantum correlations $C_{\uparrow,\downarrow} = \mathrm{cov}(\hat{n}_{\uparrow,i}, \hat{n}_{\downarrow,i})$, the staggered magnetization m_π, the magnetization m_0; with $\mathrm{cov}(\hat{X}, \hat{Y}) = \langle \hat{X}\,\hat{Y} \rangle - \langle \hat{X} \rangle \langle \hat{Y} \rangle$, $m_\theta = \sqrt{\langle |\sum_i e^{i\theta d_i} \hat{S}_{z,i}|^2 \rangle}/N_s$, $d_i = i_x + i_y$ and the lattice position $\{i_x, i_y\}, i_{x/y} \in \mathbb{Z}$. The relation between fluctuations in this limit with $V_Q > 0$, ϕ_+ or $V_Q < 0, \phi_-$ is $\Delta(\hat{n}_i)^2 = 0$, $\Delta(\hat{n}_{\uparrow\downarrow,i})^2 = 1/4$, and $C_{\uparrow,\downarrow} = -1/4$. In the case of $V_Q > 0$, and ϕ_+, the ground state is a degenerate insulator with global AFM correlations (AFM_GI) and maximal $|C_{\uparrow,\downarrow}| \neq 0$. The ground state degeneracy is $g_G^0 \sim 2^{N_s - 1/3} (N_s)^{-1/2}$, all the states with magnetization $m_0 = 0$ and one particle per site. This large degeneracy persists for small t_0 [33]. The excitation gap is $\Delta_e = \min(U, 4V_Q/N_s)$, $m_\pi \to O(N_s^{-1})$, and $n_{\rm ph} \to O(N_s^{-1})$ for $N_s \gg 1$. Surprisingly, for $V_Q < 0$ with ϕ_-, we find that a local insulating AFM state with degeneracy $g_L^0 = 2, \Delta_e = U$, maximal $m_\pi = 1$ and $n_{\rm ph} \propto N_s^2$, a staggered quantum antiferromagnet, with m_π the typical AFM order parameter. The local AFM insulating states (AFM_LI) present true conventional AFM order and nontrivial magnetic quantum correlations. In contrast, AFM_GI has only nontrivial magnetic quantum correlations. Either ground state has $\uparrow\downarrow$ components anticorrelated [33]. Thus, the many-body insulating states with $C_{\uparrow,\downarrow} \neq 0$ are $|\Psi_{\uparrow,\downarrow}\rangle \neq |\Psi_\uparrow\rangle \otimes |\Psi_\downarrow\rangle$ with the entanglement entropy between spin sectors $\mathcal{S}_\sigma \neq 0$, as we confirm below. Deep in the MI, these facts are independent of dimensionality. Away from the MI, the SF state emerges decreasing spin correlations while reaching a paramagnetic state, as $U \to 0$ then $C_{\uparrow,\downarrow} \to 0$ and $|\Psi_{\uparrow,\downarrow}\rangle \approx |\Psi_\uparrow\rangle \otimes |\Psi_\downarrow\rangle$.

Competition of magnetic configurations.—Interestingly, even if V_C is fixed by nature for a given alkali atom, modifying the pump angle and V_Q allows the competition between AFM and FM in a single setup. The emergent phases of quantum matter can be understood by analyzing the number fluctuations for $\uparrow\downarrow$ components, the total number fluctuations, $C_{\uparrow,\downarrow}$ and $\mathcal{S}_\sigma$. The information of fluctuations and correlations might be accessed via *in situ* measurements [3] or direct measurements of AFM correlations [48,49]. We perform simulations with exact diagonalization (ED) and density matrix renormalization group (DMRG) in one dimension [33,50,51]. We construct the ground state phase diagrams in Figs. 2(a)–2(d) with ED (eight sites, two spin components, and $\sim 5 \times 10^5$ states).

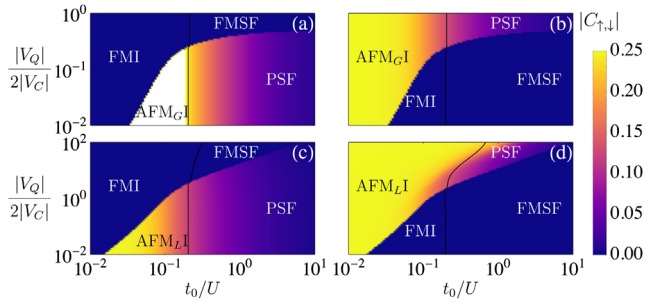

FIG. 2. Phase diagrams of magnetic configurations competition scenarios. The spin quantum correlations $|C_{\uparrow,\downarrow}|$ for V_Q (global) and V_C (local) magnetic interactions. The competition triggers QPTs between AFM $\leftrightarrow$ FM. Black lines approximate the QCP of the SF-MI QPT, where the total on-site number fluctuations are half of the limit $t_0 \gg U$, $\max[\Delta(\hat{n}_i)^2] = 1 - N_s^{-1}$. Parameters are (a) $V_C > 0$, $V_Q < 0$, ϕ_+; (b) $V_C < 0$, $V_Q > 0$, ϕ_+; (c) $V_C > 0$, $V_Q > 0$, ϕ_-; (d) $V_C < 0$, $V_Q < 0$, ϕ_-, with $N_s = 8$, two spin components, $\epsilon_{\uparrow\downarrow} = 10^{-8}U$ using ED.

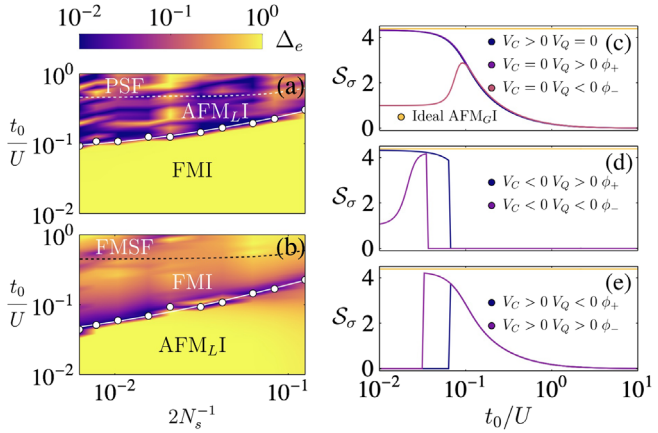

FIG. 3. Excitation gap in units of U and entanglement entropy of spin components. Panels (a), (b) Δ_e from DMRG simulations in one dimension with ϕ_-. White lines are the finite size scaling fits (FFS) for the AFM $\leftrightarrow$ FM QPT (white points). FSS for the critical t_0, $t_c \approx (a_0 + a_1 N_s^{-3/4})U$. Estimated SF-MI boundary, white (black) dashed lines (similar procedure as in Fig. 1). Parameters are $V_Q = V_C = 0.035U$, $\{a_0, a_1\} = \{0.072, 1.567\}$; (b) $V_Q = V_C = -0.03U$, $\{0.028, 1.768\}$, with maximum number of atoms per site $n_{\max} = 4$, commensurate filling $N_b = N_s$, $\epsilon_{\uparrow\downarrow} = 10^{-4}U$. Panels (c)–(e), the entanglement entropy $\mathcal{S}_\sigma$. Parameters are $V_Q \neq 0 : |V_Q|/|V_C| = 0.05$; $V_C = 0.03U, N_s = 6, \epsilon_{\uparrow\downarrow} = 10^{-8}U$ using ED.

$$\text{FMI} \leftrightarrow \text{AFMI} \leftrightarrow \text{PSF} \quad \text{or} \quad \text{AFMI} \leftrightarrow \text{FMI} \leftrightarrow \text{FMSF}.$$

Using DMRG with up to ~100 sites with two spin components and finite size scaling [33,51], we confirm a finite Δ_e that vanishes at the transition between AFM $\leftrightarrow$ FM phases in general, Figs. 3(a) and 3(b). In FM and AFM$_L$I phases $\Delta_e \sim U$. However, from the deep MI limit of AFM$_G$I, $\Delta_e \sim \min(N_s^{-1}, U)$ can be considerably smaller. In the large V_Q/U limit, $\Delta_e \sim U$. The AFM order parameter, m_π with ϕ_- decreases as Δ_e closes, for details see Ref. [33]. In general, via the cavity induced magnetic interactions it is possible to control whichever scenario one would desire.

Spin entanglement.—Typically entanglement partitioning considers spatial subsystems. However, we are interested in how the entanglement between spin projections relates to the magnetic properties of the many-body state. Therefore, we analyze by tracing over different spin projection subsystems via the entanglement entropy $\mathcal{S}_\sigma = -\text{Tr}[\rho_\sigma \log_2 \rho_\sigma]$ [52]. We find that $\mathcal{S}_\sigma$ gets maximized in the insulator region of the phase diagram for SCOL: $V_C > 0$, $V_Q = 0$, and SQOL: $V_C = 0$, $V_Q > 0$, ϕ_+ having $\max(\mathcal{S}_\sigma) = \log_2(g_G^0)$. This is the entanglement entropy of the ideal AFM$_G$I, deep in the MI, with maximal $|C_{\uparrow,\downarrow}|$. The transition is smooth due to dimensionality and finite size. Surprisingly, this is not the case for AFM$_L$I with $V_C = 0$, $V_Q < 0$, ϕ_-. The difference origins in the degeneracy of the ground states deep in the MI. Here $g_L = g_L^0 = 2$ having $\mathcal{S}_\sigma = 1$. Increasing t_0/U, non-monotonic character emerges because the ground state degeneracy increases reaching the MI-SF transition as $\Delta_e \to 0$, while $\mathcal{S}_\sigma$ maximizes. Beyond the QCP, $\mathcal{S}_\sigma$ vanishes as PSF is separable, $|\Psi_{\downarrow,\uparrow}\rangle = |\Psi_\downarrow\rangle \otimes |\Psi_\uparrow\rangle$, with $\langle \hat{n}_{\uparrow,i} \rangle = \langle \hat{n}_{\downarrow,i} \rangle \neq 0 \ \forall \ i$, Fig. 3(c).

It stands out that for $V_{C/Q} \neq 0$ with the competition between magnetic configurations, $\mathcal{S}_\sigma$ shows the first order character of the AFM $\leftrightarrow$ FM QPT, Figs. 3(d) and 3(e). These confirm that AFM and FM belong to orthogonal Hilbert space sectors. Beyond the QPT, in the FM side, $\mathcal{S}_\sigma = 0$ and $C_{\uparrow,\downarrow} = 0$, a completely polarized system with $\langle \hat{n}_{\sigma,i} \rangle \neq 0$, $\langle \hat{n}_{-\sigma,i} \rangle = 0 \ \forall \ i$. For AFM, spin entanglement and $C_{\uparrow,\downarrow}$ maximize. Moreover, QPT occurs for smaller t_0/U for ϕ_- than ϕ_+. Via $\mathcal{S}_\sigma$, it is possible to discriminate AFM$_{L/G}$ only for $V_C < 0$, Fig. 3(d).

Essentially, $\mathcal{S}_\sigma \sim 4\log_2(f(g_{L/G}))|C_{\uparrow,\downarrow}|$ for some function $f(g)$. Away from the SF-MI QCP, $\mathcal{S}_\sigma \sim 4\log_2(g_{L/G}^0)|C_{\uparrow,\downarrow}|$. The behavior of $\mathcal{S}_\sigma$ clarifies the impact of competition, degeneracy, and magnetic correlations in the ground state.

We conclude that AFM$_G$Is have more resilient entanglement accessible for sufficiently large V_Q at lower lattice depths. This could be useful as a resource for quantum state preparation (cluster states) in quantum information (QI) schemes [53,54]. This robustness could be exploited in

analog experiments to Ref. [55]. Here qubit gates with spinless neutral atoms (10^4) using the Bose-Hubbard Hamiltonian were explored.

Spinor quantum optical lattices offer great flexibility to explore the nature of different magnetic quantum phases of matter. We show that in the simplest setup, the emergence and competition of correlated antiferromagnetic or ferromagnetic quantum phases of matter can be investigated. Moreover, the system naturally supports additional competing orders via the light-induced nonmagnetic interaction terms (density wave, multimode, bond) [35,38]. Changing atomic species (i.e., rare-earth atoms [56,57]) allows other finite range interactions, density dependent tunneling processes, and peer into the landscape of Kondo physics. Using geometrically frustrated AFMs [58,59] will generate emergent degrees of freedom and possibly long-range quantum spin liquids [60–63]. It should be feasible to explore the interplay with static gauge fields [64,65] and cavity generated spin-orbit coupling via Raman transitions [66,67]. Moreover, a plethora of possibilities using dynamical gauge fields can be considered [68,69], exploring high energy physics analogs beyond local field theories.

From the QI perspective, entanglement can be tailored on demand and it is robust between spin components globally. These suggest new means to manipulate and encode information in the emergent magnetic structures found. QI and topological order [70,71] could be explored further. The combination with measurement allows dynamical order control with passive measurement setups [40,41], the inclusion of feedback protocols to tailor criticality [72–75], engineering system dynamics [76–78], and to study the interplay with time crystals [72,79–82].

We thank R. Jáuregui, D. Sahagún, I. B. Mekhov, A. Chiocchetta, F. Piazza, and T. Donner for useful discussions. This work was supported by the grants Universidad Nacional Autónoma de México (UNAM), DGAPA-PAPIIT: IN109619, UNAM-AG810720, LANMAC-2019, and CONACYT Ciencia Básica: A1-S-30934. K. L.-M. thanks the DGAPA-UNAM PAPIIT program for financial support. A. H. C. acknowledges financial support from CONACYT. We acknowledge infrastructure support for the computations from the "Laboratorio de Simulaciones Computacionales para Sistemas Cuánticos" in LANMAC (LSCSC-LANMAC) at IF-UNAM.

Note added.—Recently, we became aware of a paper [83] related to our work in dipole systems with lattices without insulators.

*scaballero@fisica.unam.mx

[1] M. Lewenstein, A. Sampera, and V. Ahufinger, *Ultracold Atoms in Optical Lattices: Simulating Quantum Many-Body Systems* (Oxford University Press, New York, 2012).

[2] P. T. Brown, D. Mitra, E. Guardado-Sanchez, P. Schauß, S. S. Kondov, E. Khatami, T. Paiva, N. Trivedi, D. A. Huse, and W. S. Bakr, Spin-imbalance in a 2D Fermi-Hubbard system, Science **357**, 1385 (2017).

[3] C. S. Chiu, G. Ji, A. Mazurenko, D. Greif, and M. Greiner, Quantum State Engineering of a Hubbard System with Ultracold Fermions, Phys. Rev. Lett. **120**, 243201 (2018).

[4] G. Salomon, J. Koepsell, J. Vijayan, T. A. Hilker, J. Nespolo, L. Pollet, I. Bloch, and C. Gross, Direct observation of incommensurate magnetism in Hubbard chains, Nature (London) **565**, 56 (2019).

[5] F. Görg, M. Messer, K. Sandholzer, G. Jotzu, R. Desbuquois, and T. Esslinger, Enhancement and sign change of magnetic correlations in a driven quantum many-body system, Nature (London) **553**, 481 (2018).

[6] F. Mivehvar, F. Piazza, T. Donner, and H. Ritsch, Cavity QED with quantum gases: new paradigms in many-body physics, Adv. Phys. **70**, 1 (2021).

[7] M. Landini, N. Dogra, K. Kroeger, L. Hruby, T. Donner, and T. Esslinger, Formation of a Spin Texture in a Quantum Gas Coupled to a Cavity, Phys. Rev. Lett. **120**, 223602 (2018).

[8] N. Dogra, M. Landini, K. Kroeger, L. Hruby, T. Donner, and T. Esslinger, Dissipation-induced structural instability and chiral dynamics in a quantum gas, Science **366**, 1496 (2019).

[9] R. Rosa-Medina, F. Ferri, F. Finger, N. Dogra, K. Kroeger, R. Lin, R. Chitra, T. Donner, and T. Esslinger, Observing dynamical currents in a non-Hermitian momentum lattice, arXiv:2108.11888.

[10] R. M. Kroeze, Y. Guo, V. D. Vaidya, J. Keeling, and B. L. Lev, Spinor Self-Ordering of a Quantum Gas in a Cavity, Phys. Rev. Lett. **121**, 163601 (2018).

[11] J. A. Muniz, D. Barberena, R. J. Lewis-Swan, D. J. Young, J. R. K. Cline, A. M. Rey, and J. K. Thompson, Exploring dynamical phase transitions with cold atoms in an optical cavity, Nature (London) **580**, 602 (2020).

[12] K. Roux, V. Helson, H. Konishi, and J. P. Brantut, Strongly correlated Fermions strongly coupled to light, Nat. Commun. **11**, 2974 (2020).

[13] K. Roux, V. Helson, H. Konishi, and J. P. Brantut, Cavity-assisted preparation and detection of a unitary Fermi gas, New J. Phys. **23**, 043029 (2021).

[14] F. Mivehvar, H. Ritsch, and F. Piazza, Cavity-Quantum-Electrodynamical Toolbox for Quantum Magnetism, Phys. Rev. Lett. **122**, 113603 (2019).

[15] B. Buča and D. Jaksch, Dissipation Induced Nonstationarity in a Quantum Gas, Phys. Rev. Lett. **123**, 260401 (2019).

[16] E. I. Rodríguez Chiacchio and A. Nunnenkamp, Dissipation-Induced Instabilities of a Spinor Bose-Einstein Condensate Inside an Optical Cavity, Phys. Rev. Lett. **122**, 193605 (2019).

[17] Z. C. Li, Q. H. Jiang, Z. Lan, W. Zhang, and L. Zhou, Nonlinear Floquet dynamics of spinor condensates in an optical cavity: Cavity-amplified parametric resonance, Phys. Rev. A **100**, 033617 (2019).

[18] J. Klinder, H. Keßler, M. Reza Bakhtiari, M. Thorwart, and A. Hemmerich, Observation of a Superradiant Mott Insulator in the Dicke-Hubbard Model, Phys. Rev. Lett. **115**, 230403 (2015).

[19] R. Landig, L. Hruby, N. Dogra, M. Landini, R. Mottl, T. Donner, and T. Esslinger, Quantum phases from competing short- and long-range interactions in an optical lattice, Nature (London) **532**, 476 (2016).

[20] L. Hrubya, N. Dogra, M. Landini, T. Donner, and T. Esslinger, Metastability and avalanche dynamics in strongly correlated gases with long-range interaction, Proc. Natl. Acad. Sci. U.S.A. **115**, 3279 (2018).

[21] P. Zupancic, D. Dreon, X. Li, A. Baumgartner, A. Morales, W. Zheng, N. R. Cooper, T. Esslinger, and T. Donner, P-Band Induced Self-Organization and Dynamics with Repulsively Driven Ultracold Atoms in an Optical Cavity, Phys. Rev. Lett. **123**, 233601 (2019).

[22] Y. Li, L. He, and W. Hofstetter, Lattice-supersolid phase of strongly correlated bosons in an optical cavity, Phys. Rev. A **87**, 051604(R) (2013).

[23] S. F. Caballero-Benitez and I. B. Mekhov, Quantum Optical Lattices for Emergent Many-Body Phases of Ultracold Atoms, Phys. Rev. Lett. **115**, 243604 (2015).

[24] N. Dogra, F. Brennecke, S. D. Huber, and T. Donner, Phase transitions in a Bose-Hubbard model with cavity-mediated global-range interactions, Phys. Rev. A **94**, 023632 (2016).

[25] Y. Chen, Z. Yu, and H. Zhai, Quantum phase transitions of the Bose-Hubbard model inside a cavity, Phys. Rev. A **93**, 041601(R) (2016).

[26] T. Flottat, L. de Forges de Parny, F. Hébert, V. G. Rousseau, and G. G. Batrouni, Phase diagram of bosons in a two-dimensional optical lattice with infinite-range cavity-mediated interactions, Phys. Rev. B **95**, 144501 (2017).

[27] J. Panas, A. Kauch, and K. Byczuk, Spectral properties and phase diagram of correlated lattice bosons in an optical cavity within bosonic dynamical mean-field theory, Phys. Rev. B **95**, 115105 (2017).

[28] L. Himbert, C. Cormick, R. Kraus, S. Sharma, and G. Morigi, Mean-field phase diagram of the extended Bose-Hubbard model of many-body cavity quantum electrodynamics, Phys. Rev. A **99**, 043633 (2019).

[29] R. Lin, L. Papariello, P. Molignini, R. Chitra, and A. U. J. Lode, Superfluid-Mott-insulator transition of ultracold superradiant bosons in a cavity, Phys. Rev. A **100**, 013611 (2019).

[30] H.-J. Chen, Y.-Q. Yu, D.-C. Zheng, and R. Liao, Extended Bose-Hubbard model with cavity-mediated infinite-range interactions at finite temperatures, Sci. Rep. **10**, 9076 (2020).

[31] C. M. Halati, A. Sheikhan, H. Ritsch, and C. Kollat, Numerically Exact Treatment of Many-Body Self-Organization in a Cavity, Phys. Rev. Lett. **125**, 093604 (2020).

[32] D. M. Stamper-Kurn and M. Ueda, Spinor Bose gases: Symmetries, magnetism, and quantum dynamics, Rev. Mod. Phys. **85**, 1191 (2013).

[33] See Supplemental Material at http://link.aps.org/supplemental/10.1103/PhysRevLett.128.080601 for additional details of the model, definitions of quantum states, details of numerical simulations and additional plots of physical quantities.

[34] W. Kozlowski, S. F. Caballero-Benitez, and I. B. Mekhov, Probing matter-field and atom-number correlations in optical lattices by global nondestructive addressing, Phys. Rev. A **92**, 013613 (2015).

[35] S. F. Caballero-Benitez and I. B. Mekhov, Bond order via light-induced synthetic many-body interactions of ultracold atoms in optical lattices, New J. Phys. **18**, 113010 (2016).

[36] F. Le Kien, P. Schneeweiss, and A. Rauschenbeutel, Dynamical polarizability of atoms in arbitrary light fields: General theory and application to cesium, Eur. Phys. J. D **67**, 92 (2013).

[37] C. Maschler, I. B. Mekhov, and H. Ritsch, Ultracold atoms in optical lattices generated by quantized light fields, Eur. Phys. J. D **46**, 545 (2008).

[38] S. F. Caballero-Benitez, G. Mazzucchi, and I. B. Mekhov, Quantum simulators based on the global collective light-matter interaction, Phys. Rev. A **93**, 063632 (2016).

[39] A. Camacho-Guardian, R. Paredes, and S. F. Caballero-Benitez, Quantum simulation of competing orders with fermions in quantum optical lattices, Phys. Rev. A **96**, 051602(R) (2017).

[40] G. Mazzucchi, W. Kozlowski, S. F. Caballero-Benitez, T. J. Elliott, and I. B. Mekhov, Quantum measurement-induced dynamics of many-body ultracold bosonic and fermionic systems in optical lattices, Phys. Rev. A **93**, 023632 (2016).

[41] G. Mazzucchi, S. F. Caballero-Benitez, and I. B. Mekhov, Quantum measurement-induced antiferromagnetic order and density modulations in ultracold Fermi gases in optical lattices, Sci. Rep. **6**, 31196 (2016).

[42] S. F. Caballero-Benitez and I. B. Mekhov, Quantum properties of light scattered from structured many-body phases of ultracold atoms in quantum optical lattices, New J. Phys. **17**, 123023 (2015).

[43] D. Nagy, G. Kónya, P. Domokos, and G. Szirmai, Quantum noise in a transversely-pumped-cavity, Phys. Rev. A **97**, 063602 (2018).

[44] S. F. Caballero-Benitez, D. A. Ivanov, T. Yu. Ivanova, and I. B. Mekhov (to be published).

[45] A. Periwal, E. S. Cooper, P. Kunkel, J. F. Wienand, E. J. Davis, and M. Schleier-Smith, Programmable interactions and emergent geometry in an atomic array, Nature (London) **600**, 630 (2021).

[46] L. de Forges de Parny and V. G. Rousseau, Phase diagrams of antiferromagnetic spin-1 bosons on a square optical lattice with the quadratic Zeeman effect, Phys. Rev. A **97**, 023628 (2018).

[47] Note that the effective single component ferromagnetic system has a degenerate manifold with $g_F \sim \sqrt{\frac{3}{2}}\exp(3\log[\frac{4}{3}]N_s)$ states and an excitation gap deep in the MI: $\Delta_e = U + V_C$, a renormalized single component Bose-Hubbard model.

[48] T. A Hilker, G. Salomon, F. Grusdt, A. Omran, M. Boll, E. Demler, I. Bloch, and C. Gross, Revealing hidden antiferromagnetic correlations in doped Hubbard chains via string correlators, Science **357**, 484 (2017).

[49] R. A. Hart, P. M. Duarte, T.-L. Yang, X. Liu, T. Paiva, E. Khatami, R. T. Scalettar, N. Trivedi, D. A. Huse, and R. G. Hulet, Observation of antiferromagnetic correlations in the Hubbard model with ultracold atoms, Nature (London) **519**, 211 (2015).

[50] J. M. Zhang and R. X. Dong, Exact diagonalization: The Bose-Hubbard model as an example, Eur. J. Phys. **31**, 591

(2010); D. Raventós, T. Graß, M. Lewenstein, and B. Juliá-Díaz, Cold bosons in optical lattices: A tutorial for exact diagonalization, J. Phys. B **50**, 113001 (2017); We have our own implementation of these methods using the "Armadillo C++" library: C. Sanderson and R. Curtin, Armadillo: A template-based C++ library for linear algebra, J. Open Source Softwaare **1**, 26 (2016).

[51] S. R. White, Density Matrix Formulation for Quantum Renormalization Groups, Phys. Rev. Lett. **69**, 2863 (1992); U. Schollwöck, The density-matrix renormalization group in the age of matrix product states, Ann. Phys. (Amsterdam) **326**, 96 (2011); We use the implementation for bosonic systems of M. Fishman, S. R. White, and E. M. Stoudenmire, The ITensor software library for tensor network calculations, arXiv:2007.14822.

[52] The reduced density matrix is $\rho_\sigma = \mathrm{Tr}_{\neq\sigma}[\rho] = \mathrm{Tr}_{-\sigma}[\mathrm{Tr}_0[\rho]]$, $\sigma \in \{\uparrow, \downarrow\}$. The partial trace is $\mathrm{Tr}_\sigma[\cdot]$, over all the lattice sites.

[53] K. Inaba, Y. Tokunaga, K. Tamaki, K. Igeta, and M. Yamashita, High-Fidelity Cluster State Generation for Ultracold Atoms in an Optical Lattice, Phys. Rev. Lett. **112**, 110501 (2014).

[54] M. Mamaev, J. H. Thywissen, and A. M. Rey, Quantum computation toolbox for decoherence-free qubits using multi-band alkali atoms, Adv. Quantum Technol. **3**, 1900132 (2020).

[55] B. Yang, H. Sun, C.-J. Huang, H.-Y. Wang, Y. Deng, H.-N. Dai, Z.-S. Yuan, and J.-W. Pan, Cooling and entangling ultracold atoms in optical lattices, Science **369**, 550 (2020).

[56] S. Baier, M. J. Mark, D. Petter, K. Aikawa, L. Chomaz, Z. Cai, M. Baranov, P. Zoller, and F. Ferlaino, Extended Bose-Hubbard models with ultracold magnetic atoms, Science **352**, 201 (2016).

[57] L. Riegger, N. Darkwah Oppong, M. Höfer, D. R. Fernandes, I. Bloch, and S. Fölling, Localized Magnetic Moments with Tunable Spin Exchange in a Gas of Ultracold Fermions, Phys. Rev. Lett. **120**, 143601 (2018).

[58] L. Santos, M. A. Baranov, J. I. Cirac, H. U. Everts, H. Fehrmann, and M. Lewenstein, Atomic Quantum Gases in Kagome Lattices, Phys. Rev. Lett. **93**, 030601 (2004).

[59] T. H. Leung, M. N. Schwarz, S.-W. Chang, C. D. Brown, G. Unnikrishnan, and D. Stamper-Kurn, Interaction-Enhanced Group Velocity of Bosons in the Flat Band of an Optical Kagome Lattice, Phys. Rev. Lett. **125**, 133001 (2020).

[60] L. Balents, Spin liquids in frustrated magnets, Nature (London) **464**, 199 (2010).

[61] C. Broholm, R. J. Cava, S. A. Kivelson, D. G. Nocera, M. R. Norman, and T. Senthil, Quantum spin liquids, Science **367**, 263 (2020).

[62] A. Chiocchetta, D. Kiese, F. Piazza, and S. Diehl, Cavity-induced quantum spin liquids, Nat. Commun. **12**, 5901 (2021).

[63] G. Semeghini, H. Levine, A. Keesling, S. Ebadi, T. T. Wang, D. Bluvstein, R. Verresen, H. Pichler, M. Kalinowski, R. Samajdar, A. Omran, S. Sachdev, A. Vishwanath, M. Greiner, V. Vuletic, and M. D. Lukin, Probing topological spin liquids on a programmable quantum simulator, Science **374**, 1242 (2021).

[64] G. Jotzu, M. Messer, R. Desbuquois, M. Lebrat, T. Uehlinger, D. Greif, and T. Esslinger, Experimental realization of the topological Haldane model with ultracold fermions, Nature (London) **515**, 237 (2014).

[65] M. Aidelsburger, M. Atala, M. Lohse, J. T. Barreiro, B. Paredes, and I. Bloch, Realization of the Hofstadter Hamiltonian with Ultracold Atoms in Optical Lattices, Phys. Rev. Lett. **111**, 185301 (2013).

[66] R. M. Kroeze, Y. Guo, and B. L. Lev, Dynamical Spin-Orbit Coupling of a Quantum Gas, Phys. Rev. Lett. **123**, 160404 (2019).

[67] S. Ostermann, H. Ritsch, and F. Mivehvar, Many-body phases of a planar Bose-Einstein condensate with cavity-induced spin-orbit coupling, Phys. Rev. A **103**, 023302 (2021).

[68] N. Goldman, G. Juzeliūnas, P. Ohberg, and I. B. Spielman, Light-induced gauge fields for ultracold atoms, Rep. Prog. Phys. **77**, 126401 (2014).

[69] L. Barbiero, C. Schweizer, M. Aidelsburger, E. Demler, N. Goldman, and F. Grusdt, Coupling ultracold matter to dynamical gauge fields in optical lattices: From flux attachment to $\mathbb{Z}_2$ lattice gauge theories, Sci. Adv. **5**, eaav7444 (2019).

[70] B. Zeng, X. Chen, D.-L. Zhou, and X. G. Wen, *Quantum Information Meets Quantum Matter-From Quantum Entanglement to Topological Phase in Many-Body Systems* (Springer, New York, NY, 2019).

[71] K. J. Satzinger *et al.*, Realizing topologically ordered states on a quantum processor, Science **374**, 1237 (2021).

[72] D. A. Ivanov, T. Yu. Ivanova, S. F. Caballero-Benitez, and I. B. Mekhov, Feedback-Induced Quantum Phase Transitions Using Weak Measurements, Phys. Rev. Lett. **124**, 010603 (2020).

[73] D. A. Ivanov, T. Yu. Ivanova, S. F. Caballero-Benitez, and I. B. Mekhov, Cavityless self-organization of ultracold atoms due to the feedback-induced phase transition, Sci. Rep. **10**, 10550 (2020).

[74] D. A. Ivanov, T. Yu. Ivanova, S. F. Caballero-Benitez, and I. B. Mekhov, Tuning the universality class of phase transitions by feedback: Open quantum systems beyond dissipation, Phys. Rev. A **104**, 033719 (2021).

[75] K. Kroeger, N. Dogra, R. Rosa-Medina, M. Paluch, F. Ferri, T. Donner, and T. Esslinger, Continuous feedback on a quantum gas coupled to an optical cavity, New J. Phys. **22**, 033020 (2020).

[76] G. Mazzucchi, S. F. Caballero-Benitez, D. A. Ivanov, and I. B. Mekhov, Quantum optical feedback control for creating strong correlations in many-body systems, Optica **3**, 1213 (2016).

[77] S. Wang and T. Byrnes, Quantum feedback control of atomic ensembles and spinor Bose-Einstein condensates, Phys. Rev. A **94**, 033620 (2016).

[78] Y. Fuji and Y. Ashida, Measurement-induced quantum criticality under continuous monitoring, Phys. Rev. B **102**, 054302 (2020).

[79] B. Zhu, J. Marino, N. Y. Yao, M. D. Lukin, and E. A. Demler, Dicke time crystals in driven-dissipative quantum many-body systems, New J. Phys. **21**, 073028 (2019).

[80] J. G. Cosme, J. Skulte, and L. Mathey, Time crystals in a shaken atom-cavity system, Phys. Rev. A **100**, 053615 (2019).

[81] H. Keßler, J. G Cosme, C. Georges, L. Mathey, and A. Hemmerich, From a continuous to a discrete time crystal in a dissipative atom-cavity system, New J. Phys. **22**, 085002 (2020).

[82] H. Keßler, P. Kongkhambut, C. Georges, L. Mathey, J. G. Cosme, and A. Hemmerich, Observation of a Dissipative Time Crystal, Phys. Rev. Lett. **127**, 043602 (2021).

[83] M. Schuler, D. De Bernardis, A. M. Läuchli, and P. Rabl, The vacua of dipolar cavity quantum electrodynamics, SciPost Phys. **9**, 066 (2020).